RSC Advances

PAPER

View Article Online
View Journal | View Issue

Cite this: *RSC Adv.*, 2017, **7**, 23977

Interesting Ag_3PO_4 concave rhombic dodecahedra: the same face with different morphologies and photocatalytic properties

Ruirui Guo,[a] Yaoting Fan[b] and Yu Tang *[a]

Received 18th February 2017
Accepted 27th April 2017

DOI: 10.1039/c7ra02026k

rsc.li/rsc-advances

Herein, a novel and interesting Ag_3PO_4 crystal with concave rhombic dodecahedra morphology (Ag_3PO_4 CRD) *via* facile wet chemical method is presented. Compared to Ag_3PO_4 with rhombic dodecahedra structure (Ag_3PO_4 RD), the Ag_3PO_4 CRD was also enclosed by {110} facets but with different geometrical shapes, formed through carving out four parallelepipeds at special junctions. The photocatalytic activity of Ag_3PO_4 CRD dramatically decreased, this was attributed to the concave nature inducing easier recombination of photogenerated holes and electrons and the reaction with organic molecules being more difficult due to space limitation and the shadow effect. The results indicated that the geometrical distribution of crystal facets could play an important role in determining photocatalytic properties.

Introduction

Photocatalysts have received great attention as environmentally friendly and efficient materials in the field of environmental protection.[1–5] Developing visible-light-driven photocatalysts has become a very active topic, such as chalcogenides, silver halide, and so on.[6–9] With a band gap of 2.36 eV, Ag_3PO_4 shows excellent, high photocatalytic activity in the degradation of organic dyes under visible light irradiation.[10] Morphology control of Ag_3PO_4 has been considered to be one of the most promising methods to improve its photocatalytic activity.[11–14] Accordingly, it is of great value to further investigate Ag_3PO_4 crystals with new morphologies and structures.

Recently, some morphologies of Ag_3PO_4 have been reported. Ye *et al.* fabricated Ag_3PO_4 rhombic dodecahedrons (RD) with only {110} facets exposed, which exhibited much higher photocatalytic activities than cubes bound by {100} facets for the degradation of organic contaminants.[10] Zheng *et al.* reported the tetrahedral Ag_3PO_4 microcrystals with exposed {111} facets showed the highest photocatalytic activity in visible light irradiation among the {111}, {110} and {100} facets.[11] It was elucidated that the excellent performance of tetrahedral Ag_3PO_4 crystals composed of {111} facets, was attributed to a high surface energy, leading to high charge carrier mobility and active surface reaction sites. More importantly, the reported Ag_3PO_4 crystals with various morphologies were obtained by adjusting internal experimental conditions such as raw materials, solvents, pH values, and additives,[15–19] which also could result in the difference of photocatalytic activity. Thus, it is valuable and necessary to investigate the Ag_3PO_4 crystals with various morphologies obtained by almost the same condition.

In our work, Ag_3PO_4 CRD and Ag_3PO_4 RD were obtained *via* a facile wet chemical method only by tuning the concentration of $NH_3 \cdot H_2O$ and H_3PO_4 (keep pH ≈ 7). With the same exposed {110} facets but different geometrical shapes, some outside faces of Ag_3PO_4 CRD were replaced by the corresponding inner faces at four special junctions. Thus, the relationships between morphologies and photocatalytic activities can be singly investigated in this situation.

Experimental

Sample preparation

Synthesis of Ag_3PO_4 RD. 106 mg silver nitrate was dissolved in 800 mL distilled water, and 0.86 mL ammonia solution (14 M) was added. After stirring for 30 min, concentrated phosphoric acid was slowly dropped into the above solution until pH ≈ 7 and the yellow precipitate was observed. Finally, the obtained yellow precipitate was washed with water several times and dried overnight.

Synthesis of Ag_3PO_4 CRD. In the above process, 106 mg silver nitrate was dissolved in 800 mL distilled water, and 3.1 mL ammonia solution (14 M) was added. After stirring for 30 min, concentrated phosphoric acid was slowly dropped into the above solution until pH ≈ 7 and the yellow precipitate was observed. Finally, the obtained yellow precipitate was washed with water several times and dried overnight.

[a]*Key Laboratory of Nonferrous Metals Chemistry, Resources Utilization of Gansu Province, State Key Laboratory of Applied and Organic Chemistry, College of Chemistry and Chemical Engineering, Lanzhou University, Lanzhou 730000, P. R. China. E-mail: tangyu@lzu.edu.cn; Fax: +86-931-8912582; Tel: +86-931-8912552*

[b]*College of Chemistry and Molecular Engineering, Zhengzhou University, Zhengzhou 450001, P. R. China*

Sample characterization

X-ray diffraction (XRD) experiments were carried out with a D/max-2400 diffractometer (Rigaku, Japan) using Cu-Kα radiation. The morphologies were examined by scanning electron microscopy (SEM, Hitachi S-4800). Diffuse reflectance ultraviolet-visible (UV-Vis) absorption spectra were measured by a PerkinElmer Lambda 950 spectrometer in the region of 200–700 nm, while $BaSO_4$ was used as a reference. Electrochemical and photoelectrochemical measurements were performed in 0.5 M Na_2SO_4 electrolyte solution in a three-electrode quartz cell, platinum wire and Ag/AgCl electrode were served as the counter electrode and reference electrode respectively. The measurements were performed on a CHI-660C electrochemical workstation. Specific surface areas were computed from the isotherms by applying the Brunauer–Emmett–Teller (BET) method using a Micromeritics ASAP 2000 system.

Evaluation of photocatalytic activity

The photocatalytic activity of samples was measured by the decomposition of Rhodamine B (RhB) solution in a reactor at room temperature. In a typical process for degradation, 200 mg of photocatalyst was suspended in the RhB solution (10 mg L^{-1}, 80 mL). Before irradiation, the suspensions were stirred for 30 min in the dark to ensure the establishment of adsorption–desorption equilibrium. A 350 W Xenon lamp equipped with an ultraviolet cutoff filter ($\lambda \geqq 420$ nm) was employed for the visible light irradiation source which was positioned 20 cm away from the reactor to trigger the photocatalytic reaction. A certain volume of suspension was withdrawn at selected times for analysis. After recovering the photocatalyst by centrifugation, the concentration of dye solution was analyzed by measuring the light absorption of the clear solution at 554 nm (λ_{max} for RhB solution) using a spectrophotometer (WFJ-7200, Unico, USA). The percentage of degradation was calculated by C/C_0. Here, C is the concentration of remaining dye solution at each irradiated time interval, while C_0 is the initial concentration.

Results and discussion

XRD patterns of Ag_3PO_4 CRD and Ag_3PO_4 RD shown in Fig. 1 indicate that all peaks of the Ag_3PO_4 can be indexed very well with JCPDS No. 06-0505, and no peaks of other impurities can be detected. Compared with Ag_3PO_4 RD, the relative intensity of the (110) peak decreases as shown in Table 1, which could be attributed to the change of the geometrical shape of two kinds of Ag_3PO_4.[20]

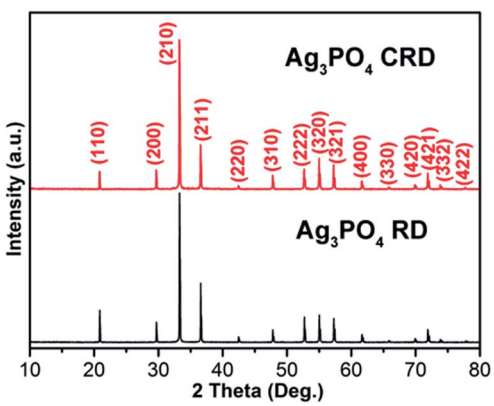

Fig. 1 XRD patterns of Ag_3PO_4 CRD and Ag_3PO_4 RD.

Table 1 Intensity ratios of XRD peaks (110)/(222) and (211)/(222) of Ag_3PO_4 CRD and Ag_3PO_4 RD

Intensity ratio	Ag_3PO_4 RD	Ag_3PO_4 CRD
(110)/(222)	1.5	1.1
(211)/(222)	2.9	2.5

Fig. 2 shows the SEM images of Ag_3PO_4 CRD and Ag_3PO_4 RD. Compared with Ag_3PO_4 RD, there are four pits at the special corners on Ag_3PO_4 CRD. Fig. 3(a1–a3) presents the geometrical shapes of the Ag_3PO_4 RD from different view. It can be seen that the Ag_3PO_4 RD consists of 12 rhombus facets and 14 junctions. Fig. 3(b1–b3) and (c1–c3) present the diamond visualization of Ag_3PO_4 RD and Ag_3PO_4 CRD from different view, respectively, and the atoms of Ag and O were hided and only P displayed in order to identify easily. Compared with Ag_3PO_4 RD, every three face at special corners on Ag_3PO_4 CRD, such as the blue site pointed in Fig. 3(a1–a3), were carving out a parallelepiped. Then, four concaves with four new inner junctions were formed and corresponding four initial outside junctions disappear, as shown in Fig. 3(c1–c3). Thus, the spacial facets of Ag_3PO_4 RD were replaced by the new inner facets in Ag_3PO_4 CRD with the same area and the same {110} facet, which is firstly reported.

Before testing the photocatalytic activity for RhB solution, the UV-Vis absorption spectra of Ag_3PO_4 CRD and Ag_3PO_4 RD were measured. As shown in Fig. 4, there is a slight difference between the samples. Ag_3PO_4 RD is able to absorb light up to approximately 535 nm, while Ag_3PO_4 CRD has an absorption edge around 520 nm. Since the size of the crystals is very similar (2 μm) and there are no signs of foreign elemental doping in the sample, it is thought that the absorption edge shift is likely to be due to the morphology transformation, which may result in the XRD peaks ratios change.[10,21] According to the previous report,[11] the band gaps of the Ag_3PO_4 {111}, {110} and {100} surfaces were calculated to be 2.736 eV, 2.613 eV and 2.032 eV, respectively.

This indicates that Ag_3PO_4 CRD with lower intensity ratios of XRD peaks (110)/(222) can be attributed to the morphology transformation, thus possesses larger band gap value, which is consisted with the blue shift of absorption edge.

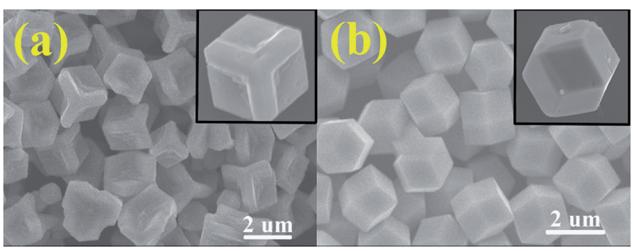

Fig. 2 SEM images of (a) Ag_3PO_4 CRD and (b) Ag_3PO_4 RD.

Using the BET method, it is turned out to be that the Ag_3PO_4 RD has a specific surface of 1.6 $m^2\ g^{-1}$ and the Ag_3PO_4 CRD is 5.91 $m^2\ g^{-1}$, respectively. According to the different morphologies of Ag_3PO_4 RD and Ag_3PO_4 CRD, it can be seen that every three face at special corners on Ag_3PO_4 CRD was carved out a parallelepiped, then every Ag_3PO_4 CRD crystal is more lighter than Ag_3PO_4 RD. So the numbers of Ag_3PO_4 CRD crystals are more than that of Ag_3PO_4 RD in the same unit mass and the surface area of Ag_3PO_4 RD was somewhat smaller than that of Ag_3PO_4 CRD, which also demonstrated that the improved catalytic activity of Ag_3PO_4 RD was not caused by the specific surface area to a certain extent.

On the basis of previous reports, the separation efficiency of electrons and holes played an important role and the photoelectrochemical parameters could be used to investigate the excitation and transfer of photo-generated charge carriers in the photocatalytic process.[22,23] To better confirm the reason why the same face with different morphology and photocatalytic properties of Ag_3PO_4 CRD and Ag_3PO_4 RD, the photocurrent responses in an electrolyte under visible light and EIS (Nyquist plot) using a three-electrode system in 0.5 M Na_2SO_4 solution were performed, which may indirectly correlate with the

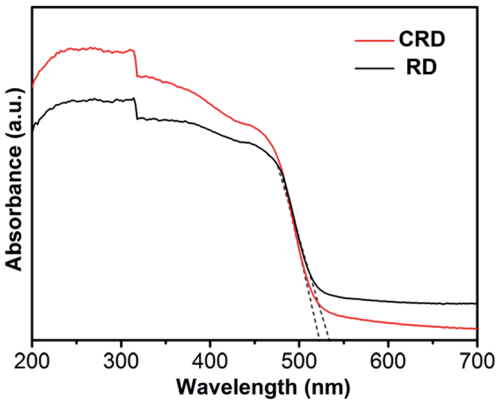

Fig. 4 UV-Vis absorption spectra of Ag_3PO_4 CRD and Ag_3PO_4 RD.

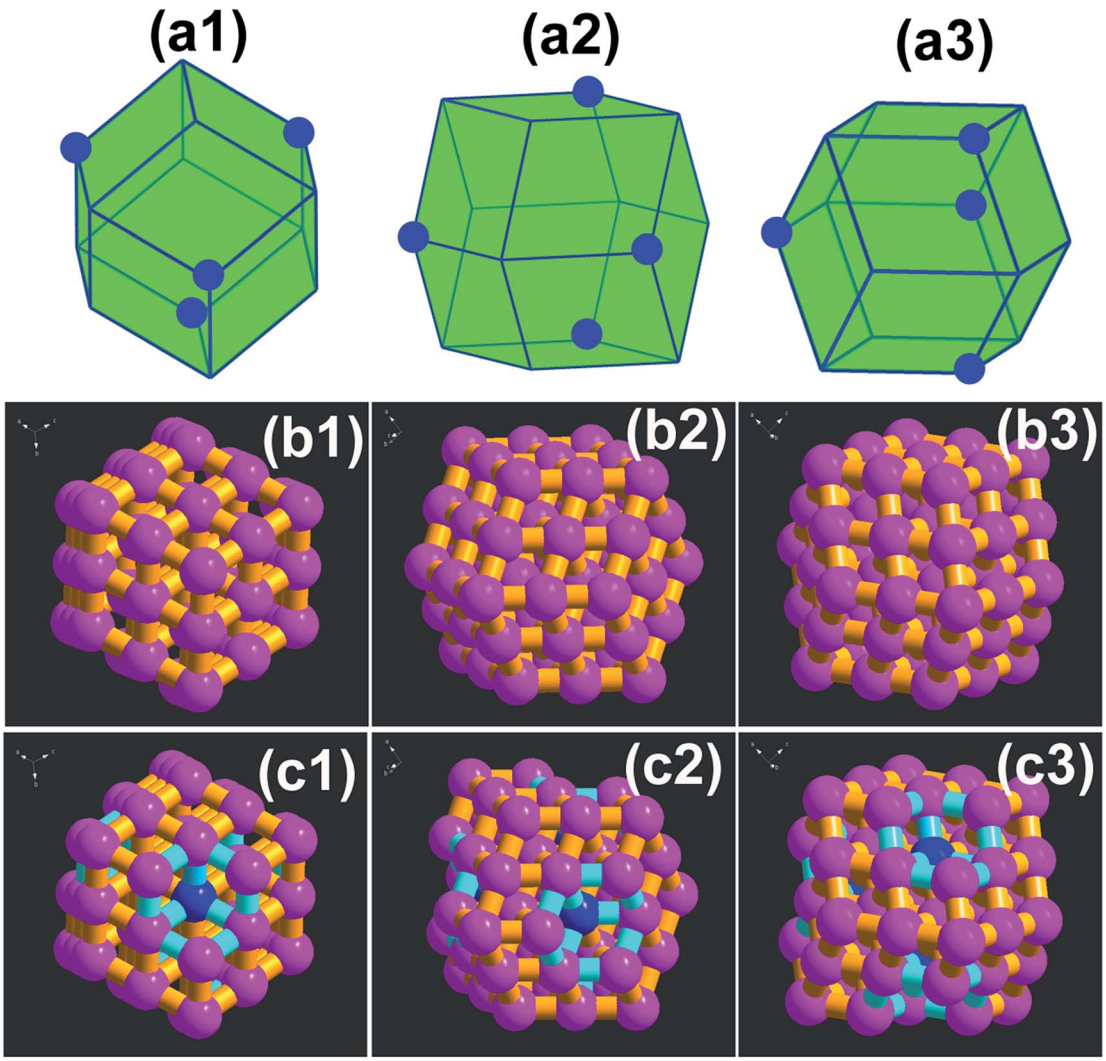

Fig. 3 (a1–a3) Geometrical shapes of the Ag_3PO_4 RD from different view; diamond visualization of (b1–b3) Ag_3PO_4 RD and (c1–c3) Ag_3PO_4 CRD from different view.

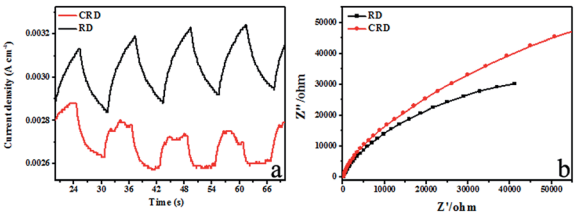

Fig. 5 Transient photocurrent of Ag_3PO_4 CRD and Ag_3PO_4 RD under visible light irradiation (a) and electrochemical impedance spectra (Nyquist plot) of Ag_3PO_4 CRD and Ag_3PO_4 RD (b).

generation and transfer to the photoinduced charge carriers in the photocatalytic process of Ag_3PO_4 CRD and Ag_3PO_4 RD. The current abruptly increased and decreased when the light source was switched on and off. Remarkably, the Ag_3PO_4 RD exhibited an obviously enhanced photocurrent response compared with Ag_3PO_4 CRD as shown in Fig. 5a, which implied that less efficient separation of the photogenerated electron–hole pairs and slow transfer of photoinduced charge carriers occurred in the Ag_3PO_4 CRD. Moreover, the EIS measurements were used to study the charge transfer and recombination proces.[24,25] As shown in Fig. 5b, the diameter of the arc radius on the EIS Nyquist plot of the Ag_3PO_4 CRD was much larger than Ag_3PO_4 RD, which indicated that the more effective separation of photogenerated electron–hole pairs and fast interface charge transfer occurred in the Ag_3PO_4 RD.[26]

The Mott–Schottky plots under dark conditions were also investigated to compare the charge carrier density of Ag_3PO_4 CRD and Ag_3PO_4 RD, which were scanned using the voltage in the range of 0–1.5 eV and the frequency of 1000 Hz. The platinum wire and Ag/AgCl electrode were served as the counter electrode and reference electrode, respectively. The positive slop of the C^{-2}–E as shown in Fig. 6 indicated that the Ag_3PO_4 RD and Ag_3PO_4 CRD belonged to n-type semiconductors.[27] By plotting $1/C^2$ *versus* E, the flat-band potential of the n-type semiconductor could be quantified from the slope, which was found to shift from 0.54 eV for the Ag_3PO_4 CRD to 0.46 eV for the Ag_3PO_4 RD, and the more negative potential shift demonstrated that the separation efficiency of charge carrier was improved in the Ag_3PO_4 RD.[28]

Over all, easier generation, more efficient separation and enhanced transfer efficiency of photogenerated electron–hole pairs could be achieved in Ag_3PO_4 RD than Ag_3PO_4 CRD for degradation of RhB under visible light irradiation.

Fig. 7 shows the photocatalytic activity of the Ag_3PO_4 CRD and Ag_3PO_4 RD for RhB degradation under visible light irradiation. It can be seen that about 63% of RhB solution was degraded in 140 min for Ag_3PO_4 RD. However, only 24% of RhB was degraded for Ag_3PO_4 CRD with the same visible light irradiation. The dramatically decrease of photocatalytic activity of Ag_3PO_4 CRD is mainly attributed to the morphology change. With the concave geometrical shapes, the recombination of photogenerated holes and electrons become easier and the reaction with organic molecules could be harder due to the space limitation and shadow effect.

In this work, holes (h^+), superoxide radicals ($^{\bullet}O^{2-}$) or hydroxyl radicals ($^{\bullet}OH$) might be active species in photocatalytic process. To further explore the major specie, radical-trapping experiments with different scavengers were performed as shown in Fig. 8. In this way, 1 mM ethylenediamine tetraacetic acid disodium (EDTA-2Na, a scavenger of h^+), 1 mM benzoquinone (BQ, a scavenger of $^{\bullet}O^{2-}$), and 1 mM tertiary butanol (t-BuOH, a scavenger of $^{\bullet}OH$) were adopted in the degradation of RhB (3.5 ppm, 80 mL), which indicated that $^{\bullet}OH$ radicals were not the dominant active species compared to no scavenger. The degradation efficiency was almost decreased completely after addition of EDTA-2Na and was decreased remarkably when the BQ added, which suggest that the h^+ was the main active specie

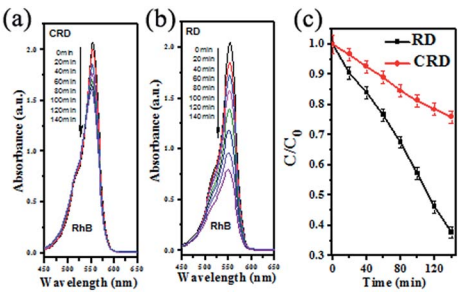

Fig. 7 Absorption of RhB aqueous solutions *versus* visible-light irradiation time in the presence of Ag_3PO_4 CRD (a) and Ag_3PO_4 RD (b); photocatalytic activity of the Ag_3PO_4 CRD and Ag_3PO_4 RD for RhB degradation under visible light irradiation (c).

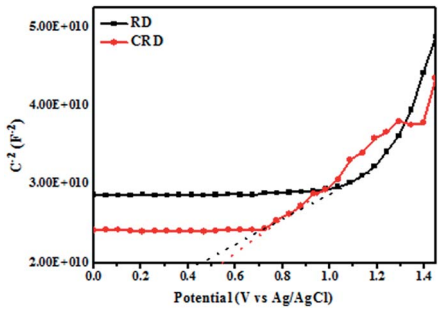

Fig. 6 Mott–Schottky plots of Ag_3PO_4 CRD and Ag_3PO_4 RD.

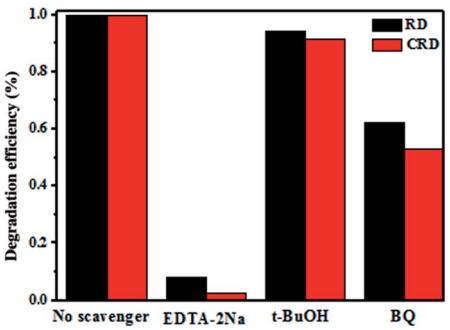

Fig. 8 Trapping experiment of active species during the photocatalytic degradation of RhB over Ag_3PO_4 CRD and Ag_3PO_4 RD under visible light irradiation.

and $^{\bullet}O^{2-}$ also played a certain role in the photocatalytic degradation of RhB solution.

Conclusion

In this work, a novel and interesting Ag_3PO_4 CRD was synthesized *via* a facile wet chemical method. Both enclosed by {110}, the Ag_3PO_4 CRD showed different geometrical shape, lower intensity ratios of XRD peaks (110)/(222), blue shift of absorption edge, less efficient separation and enhanced transfer efficiency of photogenerated electron–hole pairs compared with the Ag_3PO_4 RD. It was found that the Ag_3PO_4 CRD was formed through carving out four parallelepiped at special junctions. Furthermore, the photocatalytic activity of Ag_3PO_4 CRD dramatically decreased compared with Ag_3PO_4 RD, which was attributed to the concave nature-induced easier recombination of photogenerated holes and electrons and harder reaction with organic molecules with the space limitation and shadow effect. Apart from other reported vital factors, this work indicated that the geometrical distribution of crystal facets also plays an important role in photocatalytic property during the multielement determination.

Acknowledgements

The research leading to these results has received funding from the National Natural Science Foundation of China (Projects 21471071, 21431002).

Notes and references

1 M. Yang, N. Zhang, M. Pagliaro and Y. Xu, *Chem. Soc. Rev.*, 2014, **43**, 8240.
2 S. J. Moniz, S. A. Shevlin, D. J. Martin, Z. X. Guo and J. Tang, *Energy Environ. Sci.*, 2015, **8**, 731.
3 M. Yang and Y. Xu, *Nanoscale Horiz.*, 2016, **1**, 185.
4 H. Li, Y. Zhou, W. Tu, J. Ye and Z. Zou, *Adv. Funct. Mater.*, 2015, **25**, 998.
5 L. Zeng, X. Guo, C. He and C. Duan, *ACS Catal.*, 2016, **6**, 7935.
6 J. Hu, A. Liu, H. Jin, D. Ma, D. Yin, P. Ling, S. Wang, Z. Lin and J. Wang, *J. Am. Chem. Soc.*, 2015, **137**, 11004.
7 S. Bao, Z. Wang, X. Gong, C. Zeng, Q. Wu, B. Tian and J. Zhang, *J. Mater. Chem. A*, 2016, **4**, 18570.
8 H. Chen, G. Yu, G. D. Li, T. Xie, Y. Sun, J. Liu, H. Li, X. Huang, D. Wang, T. Asefa, W. Chen and X. Zou, *Angew. Chem., Int. Ed.*, 2016, **55**, 11442.
9 J. Ding, L. Zhang, Q. Liu, W. L. Dai and G. Guan, *Appl. Catal., B*, 2017, **203**, 335.
10 Y. Bi, S. Ouyang, N. Umezawa, J. Cao and J. Ye, *J. Am. Chem. Soc.*, 2011, **133**, 6490.
11 B. Zheng, X. Wang, C. Liu, K. Tan, Z. Xie and L. Zheng, *J. Mater. Chem. A*, 2013, **1**, 12635.
12 P. Dong, Y. Wang, H. Li, H. Li, X. Ma and L. Han, *J. Mater. Chem. A*, 2013, **1**, 4651.
13 J. Wang, S. Lou, P. Sun, L. Wang, Y. Teng, M. Chen and F. Teng, *ChemCatChem*, 2014, **6**, 2021.
14 G. Botelho, J. Andres, L. Gracia, L. S. Matos and E. Longo, *ChemPlusChem*, 2016, **81**, 202.
15 M. Li, M. Chen, J. Wang and F. Teng, *CrystEngComm*, 2014, **16**, 1237.
16 L. Wang, N. Li, Q. Zhang, S. Lou, Y. Zhao, M. Chen and F. Teng, *CrystEngComm*, 2014, **16**, 9326.
17 B. Wang, L. Wang, Z. Hao and Y. Luo, *Catal. Commun.*, 2015, **58**, 117.
18 Z. Jiao, Y. Zhang, H. Yu, G. Lu, J. Ye and Y. Bi, *Chem. Commun.*, 2013, **49**, 636.
19 U. Sulaeman, F. Febiyanto, S. Yin and T. Sato, *Catal. Commun.*, 2016, **85**, 22.
20 J. Wang, F. Teng, M. Chen, J. Xu, Y. Song and X. Zhou, *CrystEngComm*, 2013, **15**, 39.
21 H. Wang, L. He, L. Wang, P. Hu, L. Guo, X. Han and J. Li, *CrystEngComm*, 2012, **14**, 8342.
22 J. Yu, G. Dai and B. Cheng, *J. Phys. Chem. C*, 2010, **114**, 19378.
23 N. Zhang, S. Liu, X. Fu and Y. Xu, *J. Mater. Chem.*, 2012, **22**, 5042.
24 S. Yang, Y. Gong, J. Zhang, L. Zhan, L. Ma, Z. Fang, R. Vajtai, X. Wang and P. Ajayan, *Adv. Mater.*, 2013, **25**, 2452.
25 L. Huang, H. Xu, Y. Li, H. Li, X. Cheng, J. Xia, Y. Xu and G. Cai, *Dalton Trans.*, 2013, **42**, 8606.
26 L. Liu, Y. Qi, J. Lu, S. Lin, W. An, Y. Liang and W. Cui, *Appl. Catal., B*, 2016, **183**, 133.
27 P. Debabrara, K. Susanta, T. Simon, M. Mano and T. Kam, *Mater. Express*, 2011, **1**, 59.
28 I. M. P. Silva, G. Byzynski, C. Ribeiro and E. Longo, *J. Mol. Catal. A: Chem.*, 2016, **417**, 89.